Multiscale study of different types of interface of a buffer material in powder-based directed energy deposition: Example of Ti6Al4V/Ti6Al4V - Mo/Mo - Inconel 718

Amélie Thiriet[a], Catherine Schneider-Maunoury[b,c], Pascal Laheurte[a,b], Didier Boisselier[c], Laurent Weiss[a,b,*]

[a] Laboratory of Excellence for Design of Alloy Metals for Low-mass Structures ('DAMAS' Labex), Université de Lorraine, France
[b] Université de Lorraine, CNRS, LEM3, F-57000, Metz, France
[c] IREPA LASER, Parc d'Innovation Pôle API, 67400 Illkirch-Graffenstaden, France

ARTICLE INFO

Keywords:
Additive manufacturing
Microstructure
Interface
Buffer material
Micro and nano-scales

ABSTRACT

When it is difficult to deposit a material A on a material B, it is possible to create a Functionally Graded Material (FGM) using a buffer material between them to avoid the appearance of defects. The literature shows that it is very difficult, nay impossible, to have an efficient metallurgical bond between Ti6Al4V and Inconel-Mo alloys without cracks, porosities or delamination. A buffer material is therefore needed (here 25% Ti6Al4V – 75% Mo) and the fine analysis of the two interfaces thus created makes it possible to define the relevance of the choice of the buffer. Moreover, the understanding of the phenomena taking place at the interface allows the preservation of the structural integrity of a FGM made by additive manufacturing. CLAD® powder-based directed energy deposition allows the building of parts containing FGM and/or buffer materials directly during the process. The study of the interfaces at both sides of the buffer material is essential. In this paper, the first interface 100 Ti6Al4V / 25 Ti6Al4V – 75 Mo (in wt%) is smooth, suggesting that there has been diffusion between both alloys. The second one, 25 Ti6Al4V – 75 Mo / 30 Inconel 718 – 70 Mo, contains numerous exotic structures between both alloys. For such a sharp interface, we show in this paper that a microscopic study is not sufficient, but a finer scale is necessary to have a good metallurgical insight. Thus, EDS, TKD and X-ray crystallography were performed right on this interface and revealed three main structures: a hexagonal matrix, a cubic structure and an ordered hexagonal one. The hexagonal matrix appears to consist of Ni_3Ti and the ordered hexagonal one of NiMo.

1. Introduction

Additive manufacturing, and more specifically powder-based directed energy deposition, offers a wide range of possibilities concerning the geometry and the materials used. Nowadays the growing interest for custom materials has led the industry to push forward these possibilities to a whole new level: the Functionally Graded Materials (FGM) [1]. The CLAD® (Construction Laser Additive Direct) process allows the acquisition of such materials with a double powder feeder. In the same way, this technique allows the deposition of buffer materials.

The creation of interfaces between two different materials has already been studied by numerous scientific teams. Different types of materials and different mixes have been tested. From metallic alloys, for example, Yin et al. studied the additive manufacturing of Al-Ti6Al4V FGM in SLM (Selective Laser Melting) and CS (Cold Spraying) and produced samples with no intermetallics at the interfaces [3], whereas for polymers, Garcia and Prabhakar investigated the interface in polymeric additive manufacturing [4]. Different multi-material interfaces are also discussed in the review paper of Bandyopadhyay and Heer [5]. But, to our knowledge, very little information exists on the interfaces in the case of using buffer materials and, more importantly, at a micro and nano-scale.

Interfaces can be sorted in two main groups: smooth interfaces, that show good bonding (for example with diffusion, grain continuity or

* Corresponding author at: Université de Lorraine, CNRS, LEM3, F-57000 Metz, France.
E-mail address: pascal.laheurte@univ-lorraine.fr (P. Laheurte).

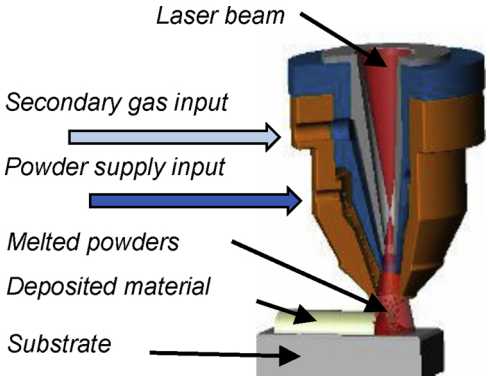

Fig. 1. CLAD® nozzle [2].

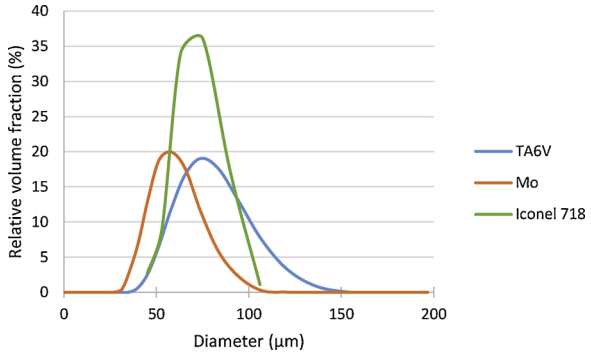

Fig. 2. Particle size distribution of TA6V, Mo and Inconel 718 powders.

good miscibility between the two materials), and sharp interfaces which form intermetallic phases, that have bad mechanical properties and tend to separate easily. For example Schneider-Maunoury et al. [6] showed that there is a good metallurgical bonding between different gradients in a Ti6Al4V-Mo alloy FGM made with CLAD®. Moreover Onuike and Bandyopadhyay [7] studied the interface between Inconel 718 and Ti6Al4V using additive manufacturing and showed that to construct a FGM with these two materials, a buffer material is needed due to numerous defects (delamination, intermetallic phases, cracking) when the two materials are directly in contact.

The main objective here is to efficiently bond Ti6Al4V, noted TA6V in this paper, with Inconel-Mo. This is practically impossible [7] so a buffer material between those two alloys is needed. An alloy containing Mo was chosen because on one hand Ti has a good solubility with Mo and on the other hand Mo is present in both TA6V-Mo and Inconel-Mo alloys so the bond between them would supposedly be satisfactory.

The aim here is to explore the interfaces 100 TA6V / 25 TA6V – 75 Mo, and 25 TA6V – 75 Mo / 30 Inconel 718 – 70 Mo (in wt%) and to show that both types of interfaces presented above can be obtained with one classic material (here 25 TA6V – 75 Mo alloy). Not only the gradients, but also these different interfaces must be taken into account when using additive manufacturing process because the latter can induce mechanical properties different from what was expected and different from the center of the gradient.

2. Materials and methods

The sample was made by CLAD® additive manufacturing process using a differential injection system in order to mix two different powders. Each material is mixed before being injected in the laser beam using a primary inert gas and is focused using a secondary inert gas flow (Fig. 1). The CLAD® process is equipped with a 2 kW laser diode with a top hat profil (λ = 980 nm, optic fiber Ø600 µm, focus point Ø 2.2 mm) and a coaxial nozzle (developed by Irepa Laser, US patent n°5418350) adapted to the high temperature conditions (> 2000∘C). The cooling system of the nozzle was modified to improve its efficiency and thus to avoid problems such as nozzle clogging and meltdown. Due to the high affinity of Ti alloys with oxygen, the machine is equipped with a gas enclosure able to maintain O2 level below 20 ppm and H2O level below 50 ppm.

Samples with dimensions of 90 mm x 4 mm x 18 mm were manufactured on a TA6V baseplate. Powders were provided by: i) TLS Technik with a particle size ranging from 45 to 90 µm for TA6V powder, ii) Tekna society with a particle size ranging from 45 to 75 µm for Mo powder and iii) LPW society with a particle size ranging from 44 to 88 µm for Inconel 718 powder. The particle size distributions of the three powders are shown in Fig. 2.

The composition of the powders presented in Table 1 are:

- TA6V powder (in wt.%): 6,21% Al + 3,97% V + 0,069% O + 0,009% N + 0,002% H + 0,2% Fe + 0,006% C + < 0,001% Y + 0,011% Cu + < 0,001% Sn + balance Ti (powder manufacturer: TLS Technik ; particles size distribution 45–90 µm),
- Mo powder (in wt.%): > 99,95% Mo + < 0,05% Ti + < 0,05% V + < 0,05% W (powder manufacturer: Teckna ; particles size distribution 45–90 µm),
- Inconel 718 powder (in wt.%): 0,65% Al + < 0,003% B + 0,05% C + 0,01% Ca + < 1% Co + 18,46% Cr + < 0,1% Cu + balance Fe + < 0,01% Mg + 0,03% Mn + 2,8% Mo + 0,02% N + 4,8% Nb + Ta + 54,52% Ni + 0,02% O + 0,012% P + < 0,005% P + < 0,005% Se + 0,15% Si + 1,01% Ti (powder manufacturer: LPW technology ; particles size distribution 44–88 µm).

Table 1
Parameters used to make the sample.

Chemical gradient	Laser power (W)	Travel speed (mm/min)	Z-increment (mm)
100% Ti6Al4V	1600	2000	0,8
25% Ti6Al4V - 75% Mo	2000	1500	0,8
30% Inconel 718 - 70% Mo	2000	1500	0,8

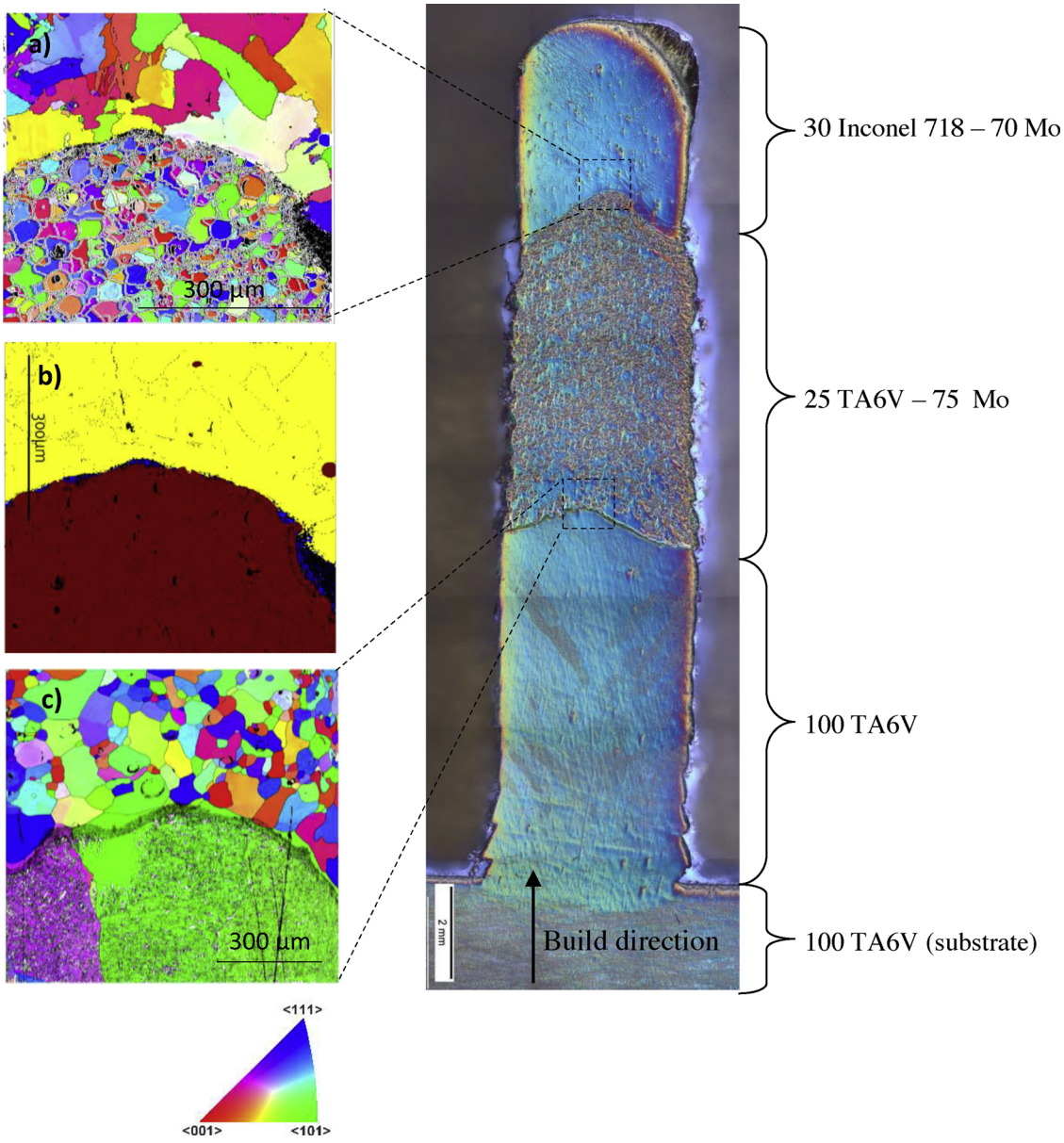

Fig. 3. EBSD maps of the interfaces of the sample. a) 25 TA6V – 75 Mo / 30 Inconel 718 – 70 Mo interface, b) Phase map of the 25 TA6V – 75 Mo / 30 Inconel 718 – 70 Mo interface (brown and yellow: cubic, blue: hexagonal), c) 100 TA6V (beta grains reconstructed with Merengue 2) / 25 TA6V – 75 Mo interface. (For interpretation of the references to colour in this figure legend, the reader is referred to the online version of this article) (For interpretation of the references to colour in this figure legend, the reader is referred to the web version of this article).

The process parameters such as the laser power and the travel speed were adjusted depending of the chemical composition. Table 1 show the parameters used for the sample:

DED-CLAD® process used a focused beam on the substrate. Working distance and focus point at 12.5 mm. The nozzle (US Patent 54183501) has been develop for the CLAD® additive manufacturing process which consists in injecting metallic powder under a focused laser beam.

The process parameters are as follows:

- Laser diode characterized by a laser beam diameter of 600 µm and a wavelength of 980 nm,
- Carrier gas and shielding gas: argon,
- Step-over between track: zero (single track width sample).

The studied part was obtained by cutting a slice of about 0.5 cm in the height of the sample. It was then polished on one surface and etched with a Kroll solution (mix of 2 mL of hydrofluoric acid, 5 mL of nitric

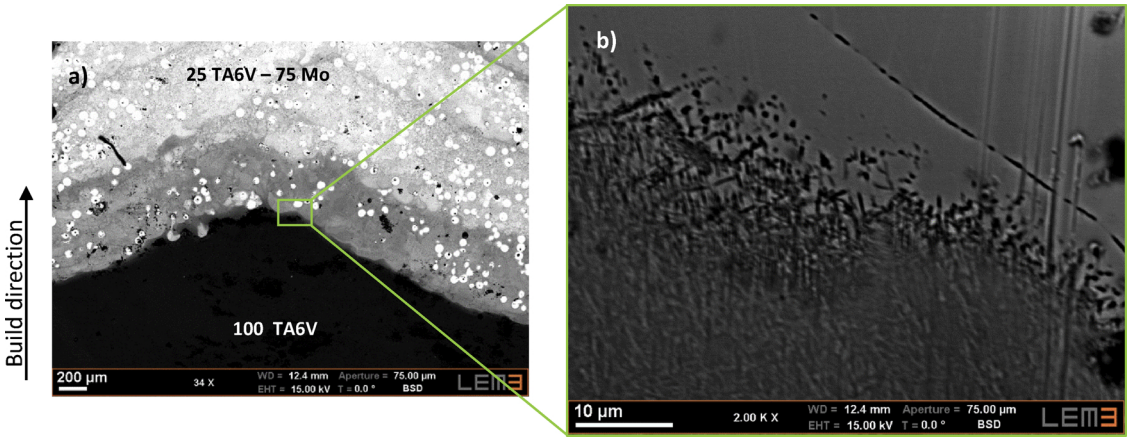

Fig. 4. Electronic images of the 100 TA6V / 25 TA6V – 75 Mo interface.

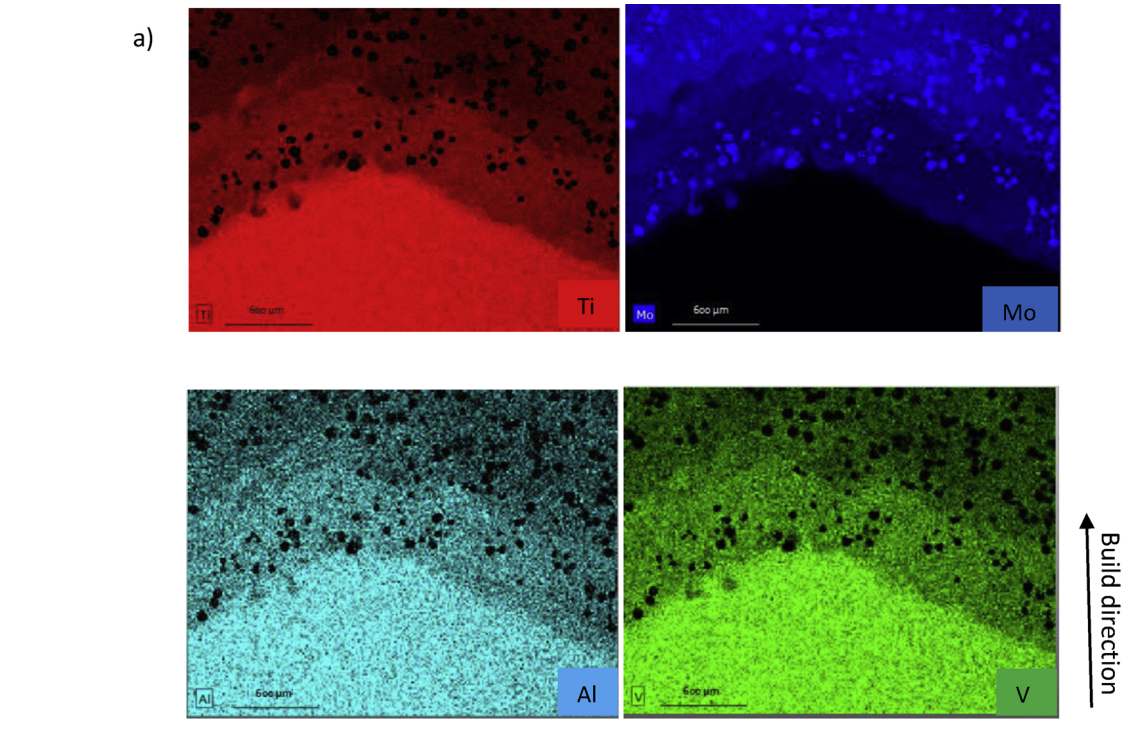

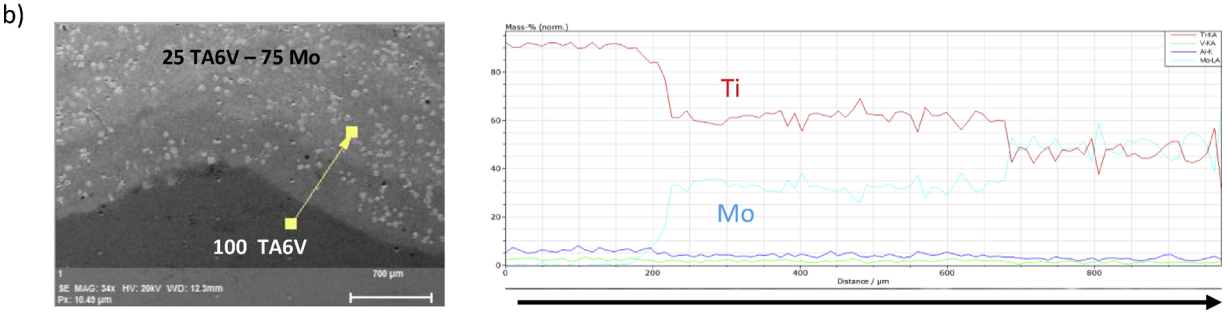

Fig. 5. a) EDS maps of the 100 TA6V / 25 TA6V – 75 Mo interface and b) line scan of the same interface.

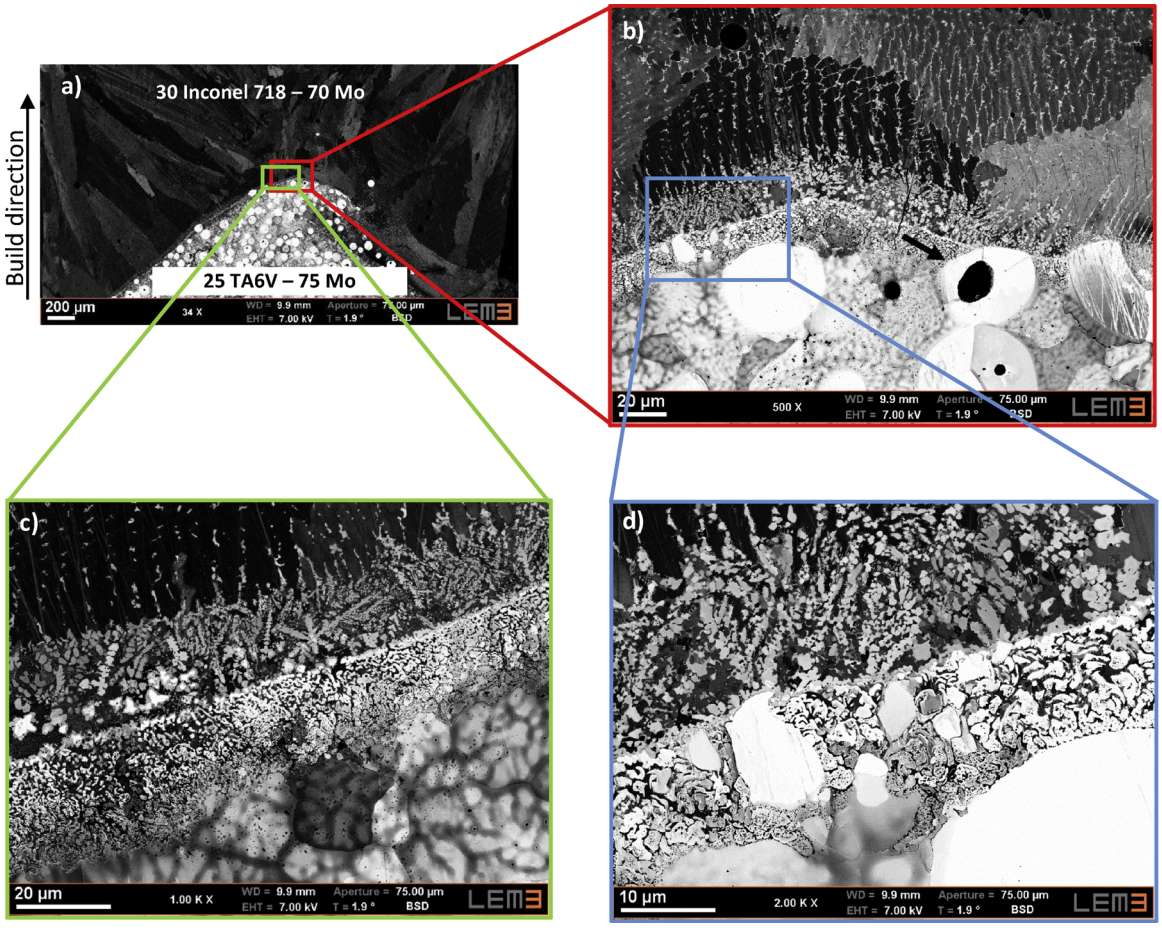

Fig. 6. Electronic images of the 25 TA6V – 75 Mo / 30 Inconel 718 – 70 Mo interface.

acid and 100 mL of water). Next, it was studied using optical imaging (Olympus BX61 with an Olympus UC30 camera), EBSD (Jeol 6490 SEM with a high-speed EBSD camera Oxford under a 20 kV voltage, about 20 mm of working distance and a tilt of 70°) reconstructed when necessary with Merengue 2 software and studied with Atex software [8], EDS (Zeiss Supra 40 SEM with a Bruker EDS detector under a 15 kV voltage and about 10 mm of working distance), electronic imaging (Zeiss Supra 40 SEM).

The thin section was cut (Zeiss Auriga FIB-SEM) in the area of the 25 TA6V – 75 Mo / 30 Inconel 718 – 70 Mo interface and studied in TKD (Zeiss Supra 40 SEM with a Bruker e-Flash HR EBSD camera and an Optimus on-axis TKD head) and XRD (D8 Advance Bruker XRD machine using the K_α wavelength of Co with a poly-capillary collimator of 1 mm diameter, a Fe K_β filter, a photonic Science plane detector and a glass cover).

3. Results and discussion

The studied sample contains 3 gradients on a TA6V substrate. The first gradient is made of 100 TA6V, the second one is a mix between 25 of TA6V and 75 of Mo, the last one contains 30 of Inconel 718 and 70 of Mo (in % wt).

3.1. Electron backscatter diffraction (EBSD) mapping

First of all, EBSD mapping was performed on each interface of the sample. The obtained maps are shown in Fig. 3 according to the build direction $< 100 >$.

TA6V ($\alpha + \beta$), during rapid cooling, transforms into martensite from high temperature β grains. The Burgers orientation rules allow the reconstruction of the β parent grains knowing the orientation of the martensite needles. By doing so, it is possible to see an excellent continuity on the 100 TA6V / 25 TA6V – 75 Mo interface (Fig. 3c)). Indeed parts of the β grains in the 100 TA6V gradient are found in the following gradient, which shows a good metallurgical bond between the two gradients.

The second interface, 25 TA6V – 75 Mo / 30 Inconel 718 – 70 Mo (Fig. 3a)), is totally different: it is sharp and there is no continuity between the two alloys. The phase map of the interface (Fig. 3b)) gives an additive and an unexpected information: right between the two β

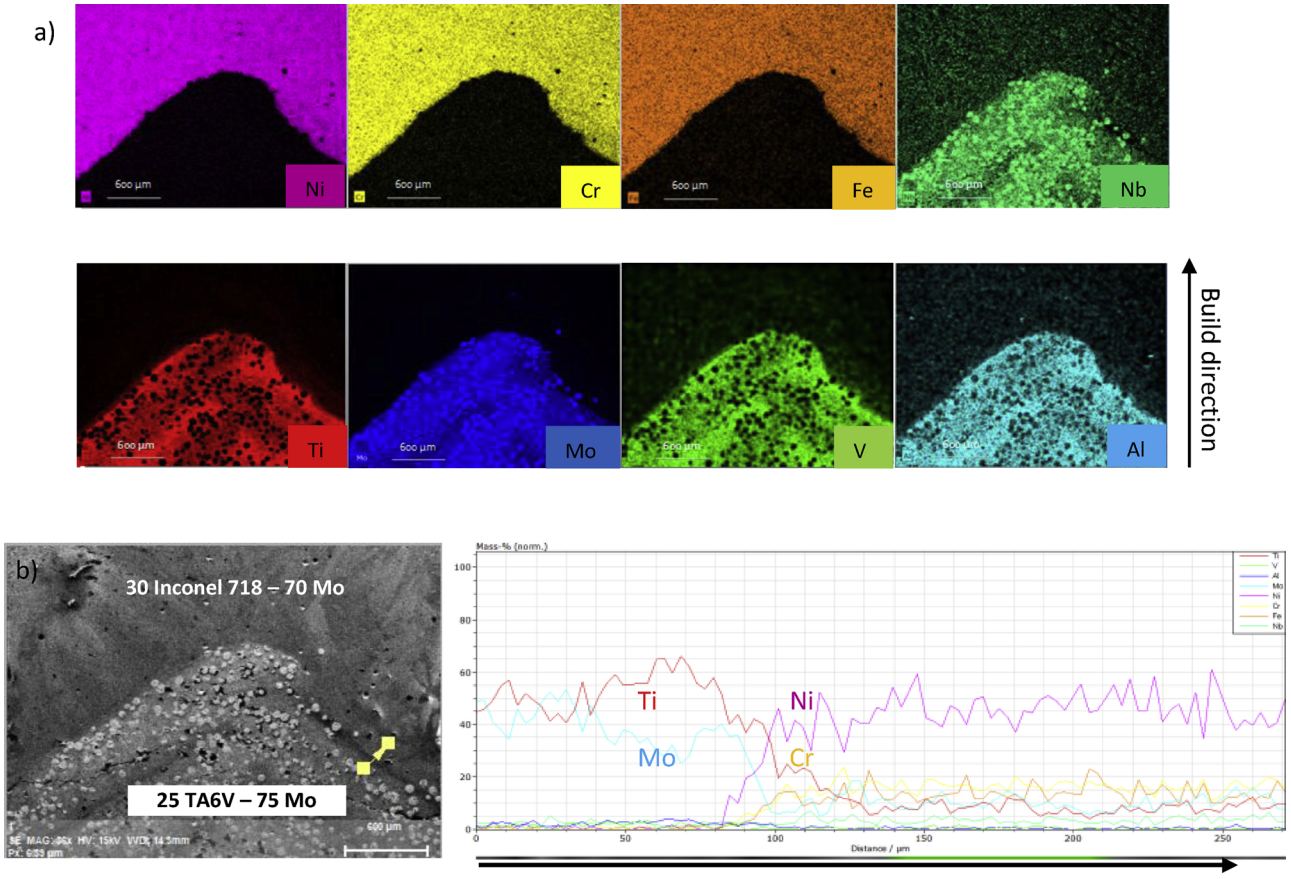

Fig. 7. a) EDS maps of the 25 TA6V – 75 Mo / 30 Inconel 718 – 70 Mo interface and b) line scan of the same interface.

phase alloys (cubic structure) a hexagonal structure is detected. This result is unexpected because given the composition, the equivalent Mo is extremely high, so the structure should be cubic, which it is not the case, as will be seen below.

3.2. Interface 100 TA6V / 25 TA6V – 75 Mo

3.2.1. Electronic imaging (SEM)

Fig. 4 shows that the interface is very short, the two alloys blend together on the interface. Very thin needles of TA6V are visible which tend to mix with the TA6V-Mo mix at the interface front, giving a rather smooth connection between the two alloys. No exotic phase is seen.

3.2.2. Energy-dispersive X-ray spectroscopy (EDS) mapping

The color gradient visible on Fig. 5a) from the TA6V to the TA6V-Mo mix and the smooth decreasing curve of Ti and increasing curve of Mo from Fig. 5b) show a chemical gradient between the two alloys: the TA6V alloy from the bottom deposited material has diffused in the TA6V-Mo mix (on about 600 µm). This allows a good metallurgical bond between the two alloys. The presence of unmelted particles will be detailed in the following sections.

3.3. Interface 25 TA6V – 75 Mo / 30 Inconel 718 – 70 Mo

3.3.1. Electronic imaging (SEM)

Fig. 6a) shows unmelted particles of Mo on the 25 TA6V – 75 Mo side (arrow). These unmelted particles can be explained by the low vaporization temperature of Ti (3560 K) of which ionized gas masks the laser beam. The power loss prevents the Mo, of which the melting temperature (2896 K) is much higher than that of Ti (1941 K), from melting. Fig. 6b) points out the presence of porosities inside some unmelted particles. These porosities were already in the initial powder.

Three main areas are visible on Fig. 6: a dendritic area on the Inconel 718-Mo side, an area composed of structures similar to intermetallics (in the middle, Fig. 6d),) and, more in depth in the TA6V-Mo mix, cells. This interfacial organization is peculiar because it contains structures appearing with both high (dendrites, on the Inconel 718-Mo side) and low (cells, Fig. 6c), on the TA6V-Mo side) cooling speeds, apart from each other by only about a few tenth of microns.

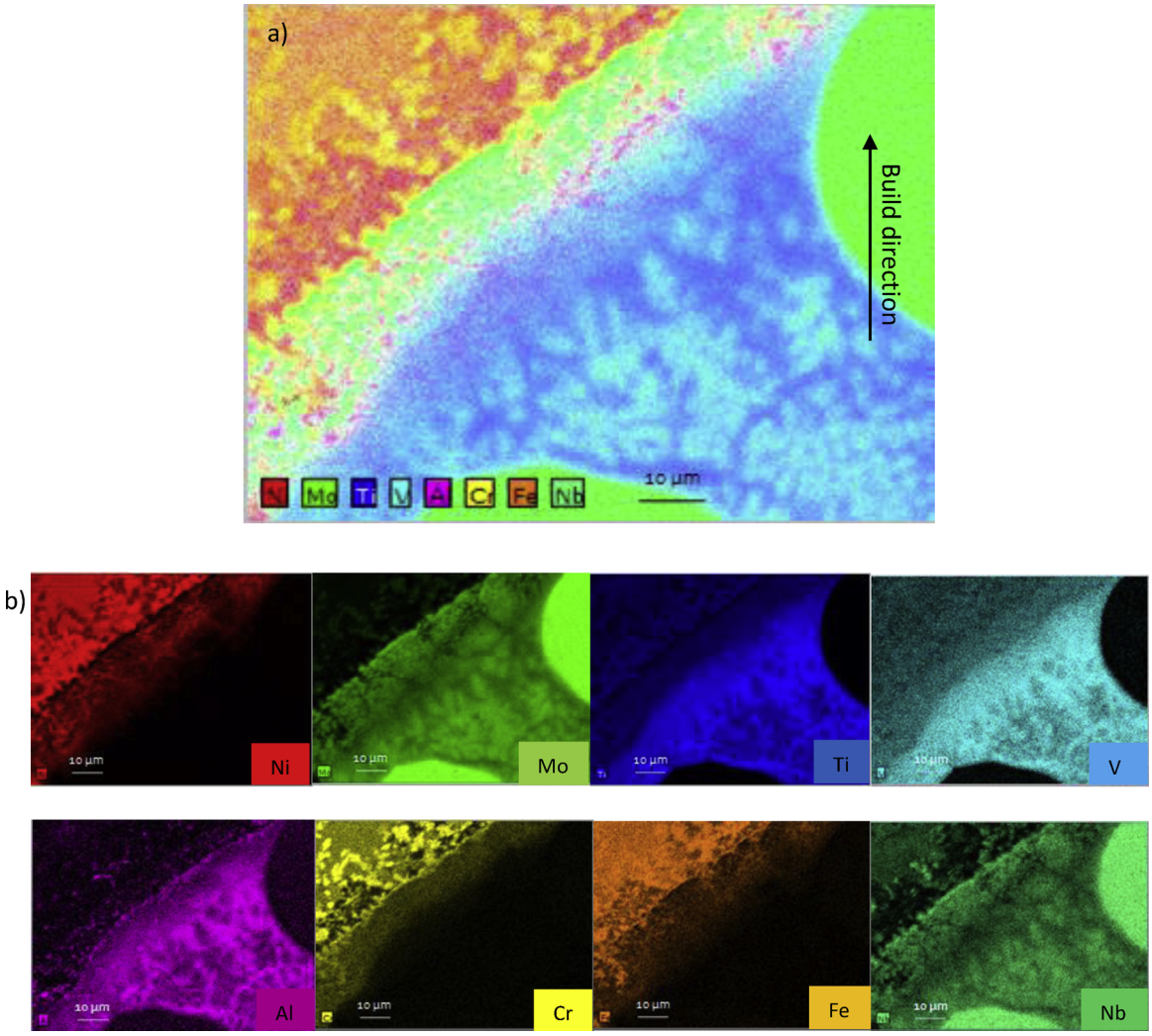

Fig. 8. EDS zoom on the 25 TA6V – 75 Mo / 30 Inconel 718 – 70 Mo, a) with all detected elements, b) for each element.

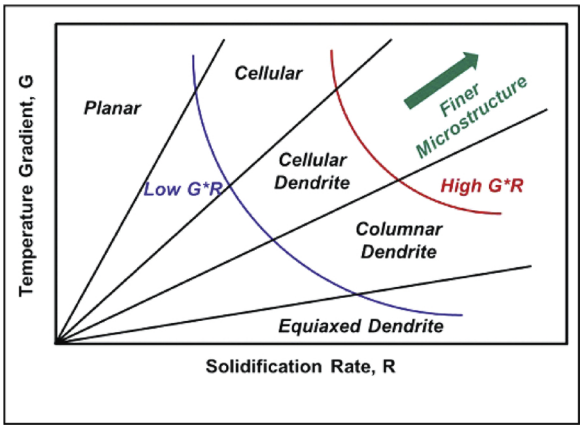

Fig. 9. Effect of the temperature gradient and the solidification rate on the solidification morphology [10].

3.3.2. Energy-dispersive X-ray spectroscopy (EDS) mapping

This interface (Fig. 7) is totally different from that of the 100 TA6V / 25 TA6V -75 Mo. It is sharp and there is no blending between the two alloys, or at least in an extremely narrow area. Note that unmelted particles of pure Mo are detected as Nb because the wavelengths of the characteristic emission lines of Mo and Nb are very close. Furthermore it should be noted that in CLAD® (Schneider-Maunoury et al. [6]) or SLM (Vrancken et al. [9]) unmelted particles of Mo are always found in TA6V-Mo mixtures.

An EDS zoom (Fig. 8) gives an approximate identification of the structure of Fig. 6. The area composed of structures similar to intermetallics contains mainly Mo. The dendrites are made of Cr surrounded by Ni and Fe and there is a chemical segregation within the cells, indicated by the TA6V encapsulating Mo. The difference in microstructure could be explained by the difference in cooling speed, linked to the thermal conductivities ($\lambda_{TA6V} = 6.7\,W\,m^{-1}\,K^{-1}$, $\lambda_{Ti} = 21.9\,W\,m^{-1}\,K^{-1}$, $\lambda_{Mo} = 138\,W\,m^{-1}\,K^{-1}$, $\lambda_{Inconel\ 718} = 11.2\,W\,m^{-1}\,K^{-1}$, $\lambda_{Ni} = 90.7\,W\,m^{-1}\,K^{-1}$ $\lambda_{Cr} = 93.7\,W\,m^{-1}\,K^{-1}$ $\lambda_{Fe} = 80.2\,W\,m^{-1}\,K^{-1}$).

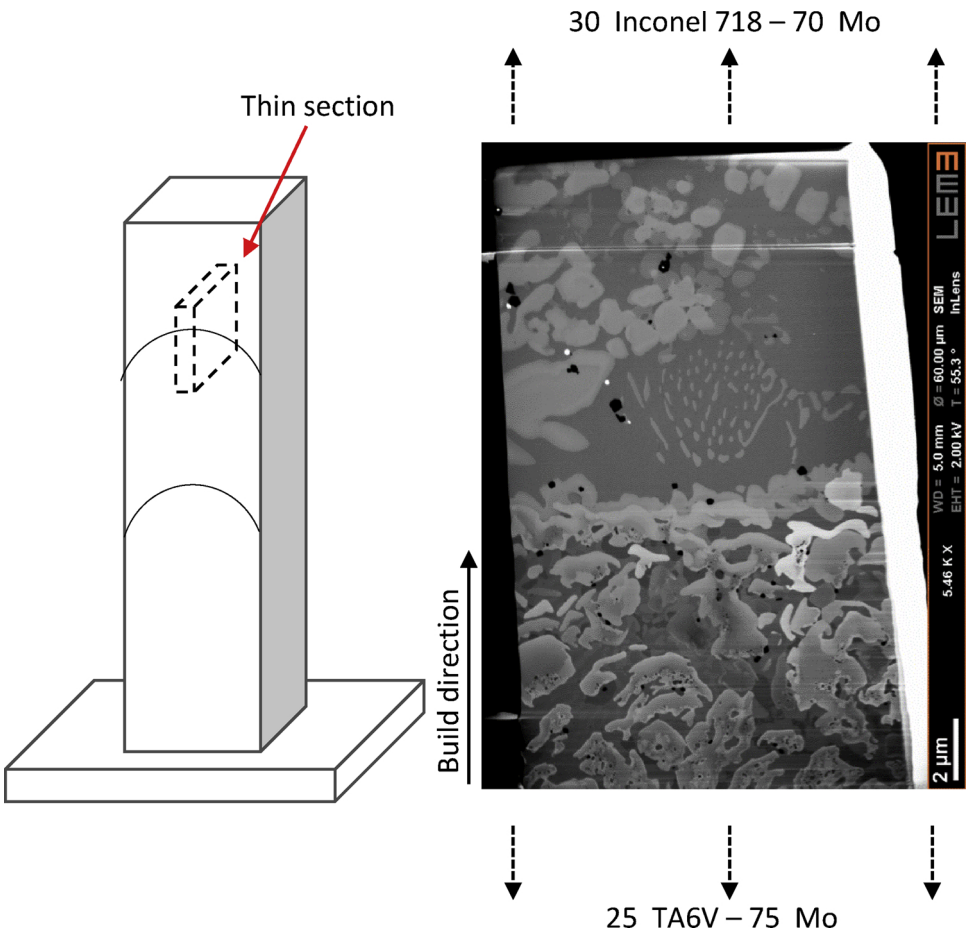

Fig. 10. Thin section of the 25 TA6V – 75 Mo / 30 Inconel 718 – 70 Mo.

Indeed, Fig. 8 shows that the elements are not anymore totally mixed on the interface. The thermal conductivities for Ni, Cr, Fe and Mo (chosen because they are the main elements on the Inconel 718-Mo side) are high. Thus, the thermal gradient is low. Taking into consideration that the solidification rate is medium to high due to the process, the solidification morphology tends to be dendritic (Fig. 9). Moreover, on the TA6V-Mo side, a hypothesis can be advanced: the Mo solidifies first. The Ti would absorb the heat from the Mo because Mo well conducts heat thanks to its high thermal conductivity. Therefore the Ti and more generally the TA6V-Mo mix would stay warm for a longer time thus would have a lower solidification rate with a medium temperature gradient and would solidify into cells.

3.4. Sub-micrometric study of the cross section of the 25 TA6V – 75 Mo/30 Inconel 718 – 70 Mo interface

A thin section was cut right on this interface (Fig. 10). On this thin section, the dendrites (on the Inconel 718-Mo side) and the intermetallics (on the TA6V-Mo side) can be seen. Yet an intermediate zone is visible between these two substructures, that appears to consist of a matrix containing small particles. Moreover the black dots observed all along the thin section are not porosities, but another phase.

A video showing the microstructure through the thin section (Fig. 10) using FIB tomography is available on the online version of this article.

3.4.1. Transmission Kikuchi diffraction (TKD)

Some dislocations are visible on Fig. 11a)) in the cubic cell structure (purple lines, white arrows), probably due to the internal stress caused by the building of the sample or the subsequent cooling.

TKD (Fig. 11) shows that there are three main substructures with different densities: a hexagonal matrix, a cubic substructure and an ordered hexagonal substructure (Fig. 12). This third substructure is composed of Ni and Mo and its apparition is genuinely possible as the heat of mix for a statistically ordered Ni and Mo liquid at the equiatomic composition is −7 kJ/mol [11].

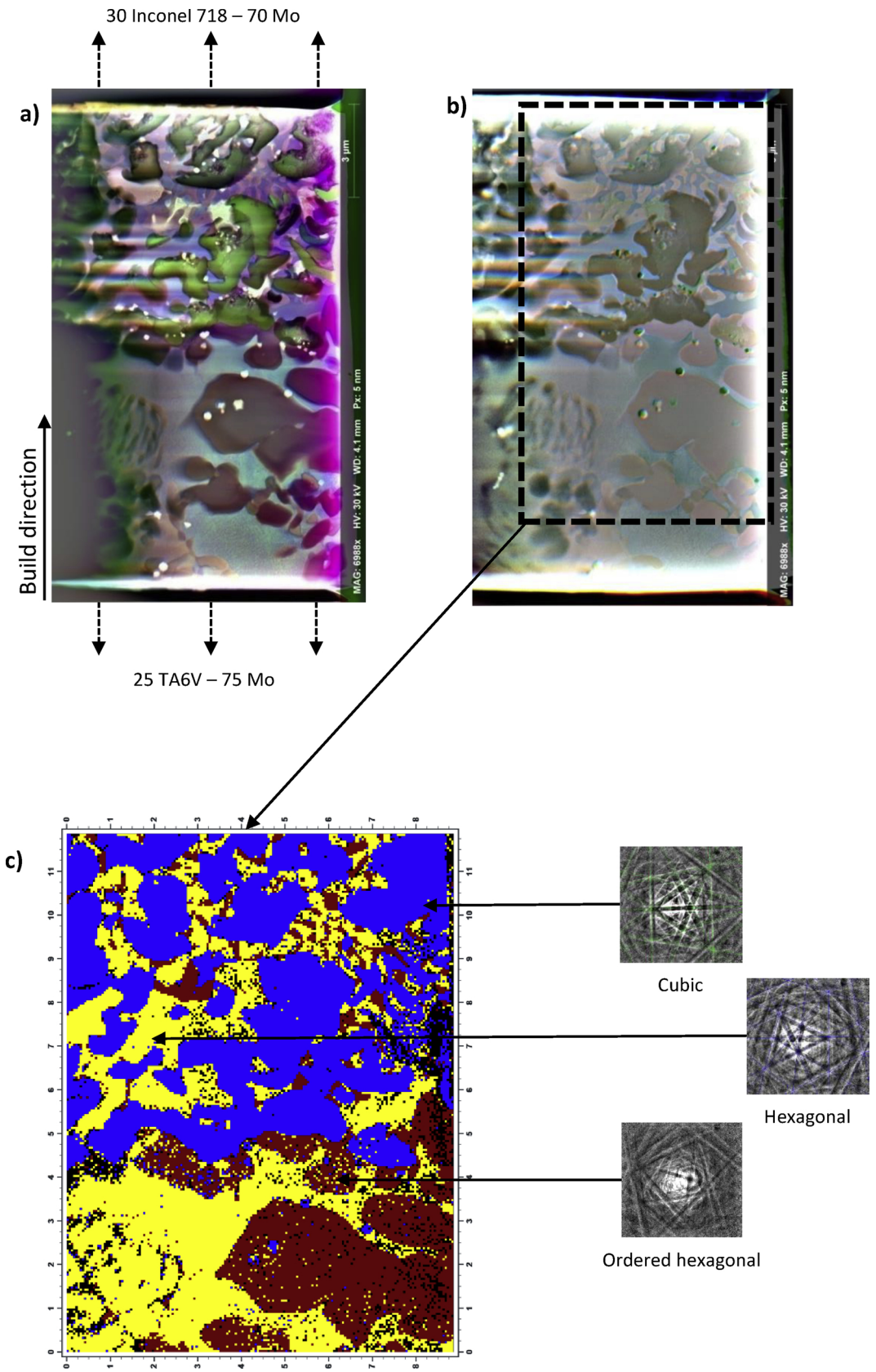

Fig. 11. TKD maps of the 25 TA6V – 75 Mo / 30 Inconel 718 – 70 Mo interface, a) FSD, b) Density contrast, c) Phase contrast (blue: cubic, yellow: hexagonal, brown: ordered hexagonal) (For interpretation of the references to colour in this figure legend, the reader is referred to the web version of this article).

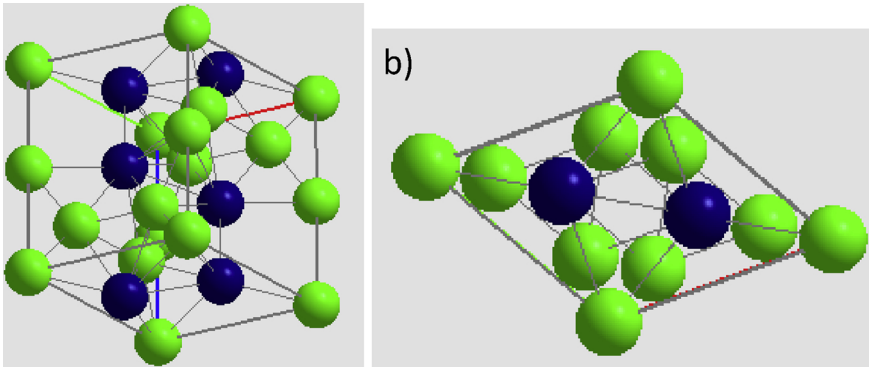

Fig. 12. NiMo ordered hexagonal cell, blue: Mo, green: Ni, a) 3D, b) top view (For interpretation of the references to colour in this figure legend, the reader is referred to the web version of this article).

3.4.2. EDS on the thin section

The EDS maps of the thin section (Fig. 13) allow the understanding of the different structures seen on this interface. First of all, the structures on the Inconel 718-Mo side (on the right on Figs. 10 and 11) are mainly composed of Mo in a Ni matrix. The ordered hexagonal structure (on the right here, on the left on Figs. 10 and 11) is predominantly made of Mo, Fe and Cr. These elements do not exclude a NiMo (circled in blue on Fig. 14c)) ordered hexagonal cell because those maps are not quantitative, they simply show a relative distribution between the elements. This structure is surrounded by a matrix with a majority of Ni. The ternary diagrams Cr-Mo-Ni and Mo-Ni-Ti (Fig. 14) show the possible existence of cubic and hexagonal cells (fcc, bcc and δ, circled in green on Fig. 14a&b)) and thus do not exclude the possibility of NiMo forming. Finally, the hexagonal matrix seen in TKD could be Ni_3Ti (circled in red on Fig. 14c)) [14]. Contrary to Onuike and Bandyopadhyay [7], who that found that a layer of Vanadium Carbide prevents the formation of intermetallics, the presence of Mo in the mixture does not prevent such an emergence. This result could also be explained by the difference of scale of the studies.

3.4.3. X-ray crystallography (XRD)

The X-ray diffraction (Fig. 15) corroborates the results obtained in EDS and TKD because a hexagonal structure close to Ni_3Ti is determined: $(Nb_{0.03}\ Ti_{0.97})Ni_3$. The NiMo structure could not be checked because not existing in our database.

Moreover, some peaks can be mixed with the background signal because of the limited size of the phases seen in the thin section.

As a matter of fact, the intermetallics located at this interface could lead to defects because of a stress field developed when solidifying, as showed Shah et al. [15] with direct laser deposition of TA6V and Inconel 718, increased by the many unmelted particles.

4. Conclusion

The two main factors to obtain an efficient metallurgical bond (no cracks, porosities or delamination) is to choose a buffer material which favors diffusion between the alloys (deep diffusion area) and avoid parasitic phases formation at the interface (small intermetallics for example). The use of a buffer material in additive manufacturing can be a solution when assembling two different alloys but it can lead to different issues on the interfaces and distinct types of microstructures even within the same sample. In the case of the studied sample, the two analyzed interfaces contain structures extremely different from each other.

(1) EBSD, EDS mapping and electronic imaging on the TA6V/TA6V-Mo interface showed that it is smooth with a grain continuity and diffusion between the two constitutive materials.
(2) Macro-scale EBSD and EDS mapping showed that the other interface, TA6V-Mo/Inconel 718-Mo, is sharp with a visible junction.
(3) Micro-scale EDS mapping and electronic imaging on the same interface (25 TA6V – 75 Mo / 30 Inconel 718 – 70 Mo) showed that there are at least three distinct structures in this area.
(4) A thin section was cut right on this interface and analyzed with nano-scale TKD, EDS and X-ray crystallography that revealed an exceptionally rich area containing various substructures such as cubic, hexagonal and ordered hexagonal phases.

Cooling speed rates are different for each element and do highly influence the microstructure during cooling down. Particularly in samples containing buffer materials, the mixing of the constituent elements at the interface must be taken into account because their different properties (for example the thermal conductivity) yield different structures.

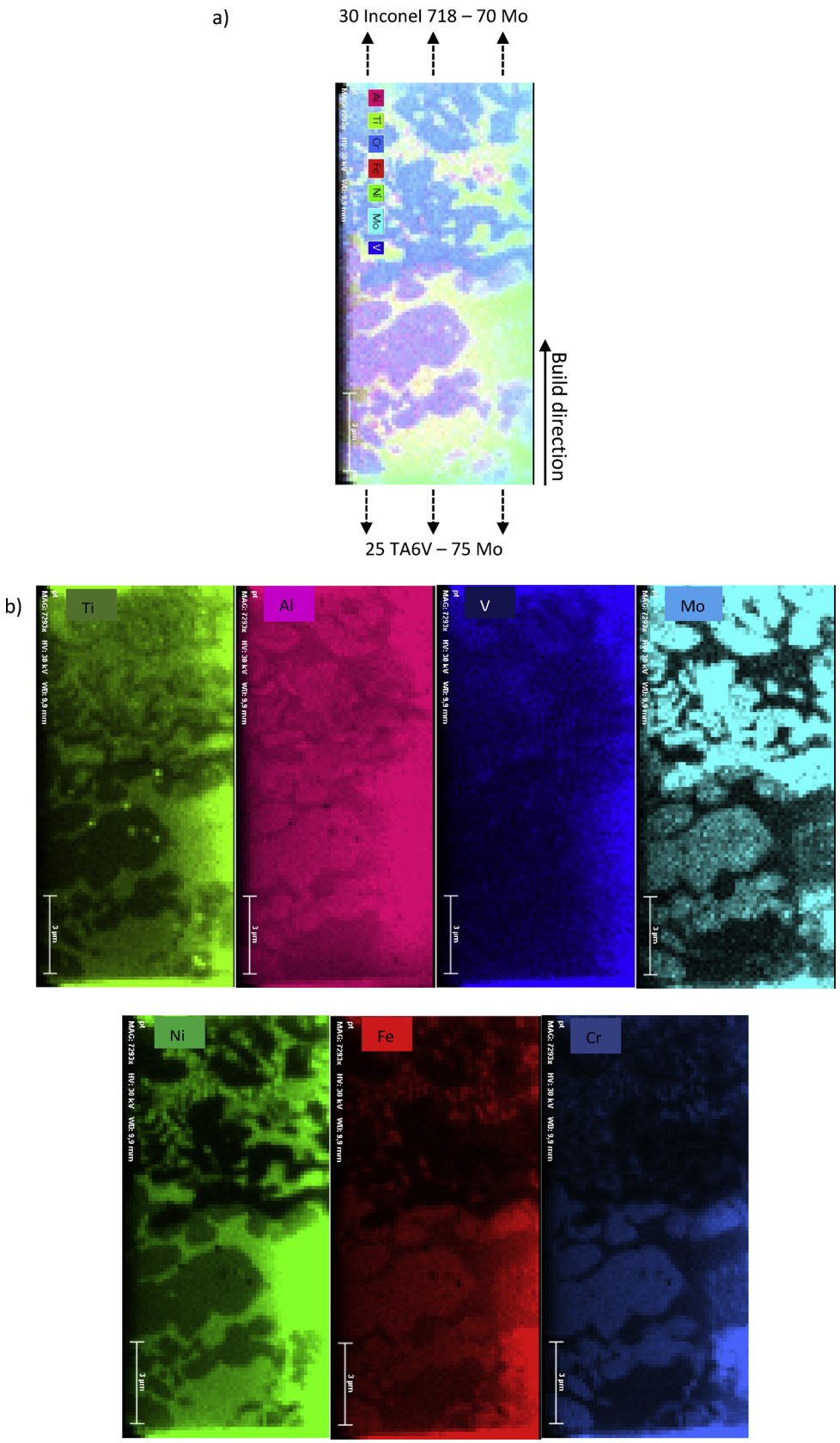

Fig. 13. EDS maps of the thin section, a) with all the detected elements, b) for each element.

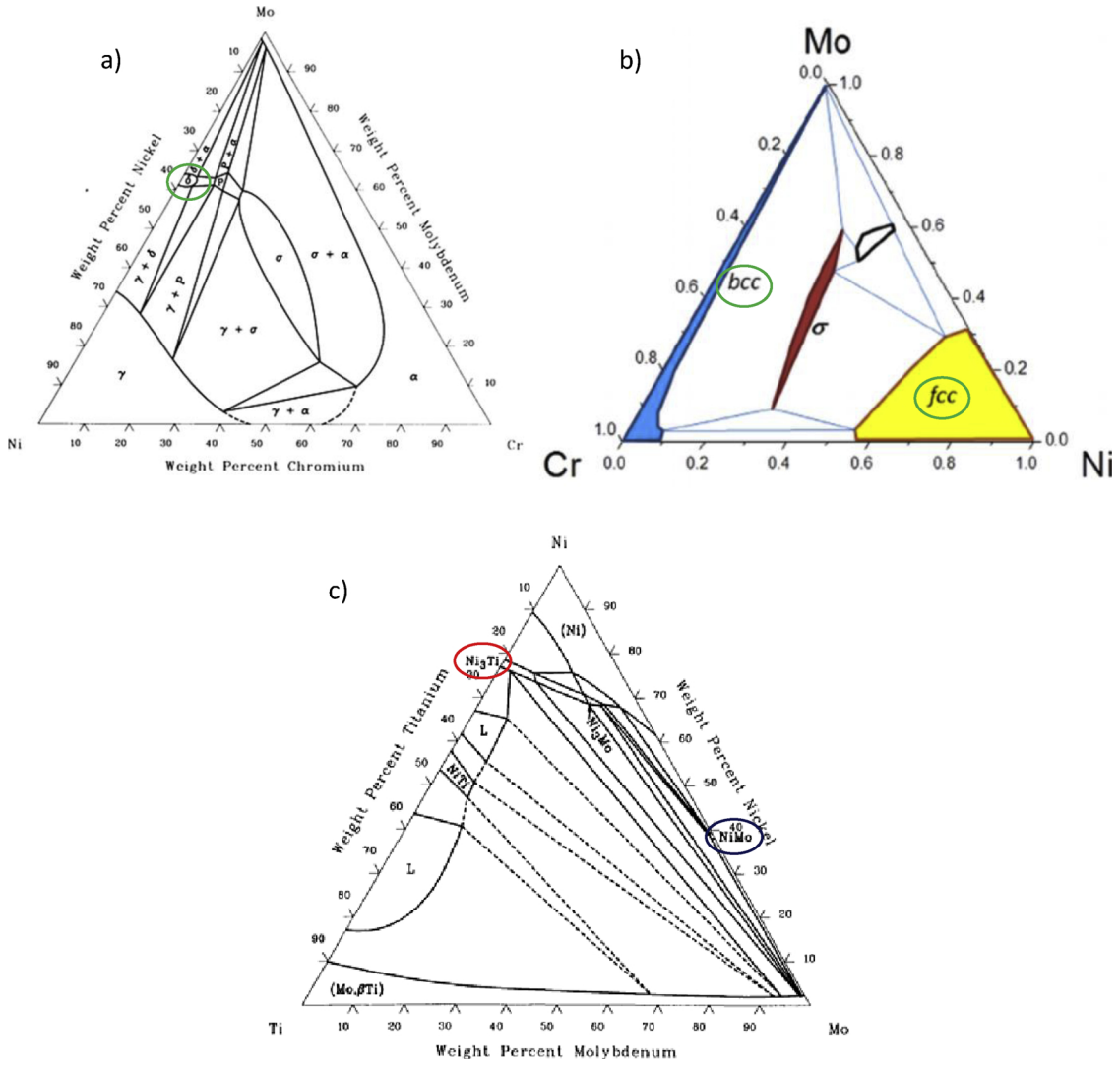

Fig. 14. Ternary diagrams, a) Cr-Mo-Ni at 1250 °C [12], b) Cr-Mo-Ni at 1050 °C [13], c) Mo-Ni-Ti at 1200 °C [12].

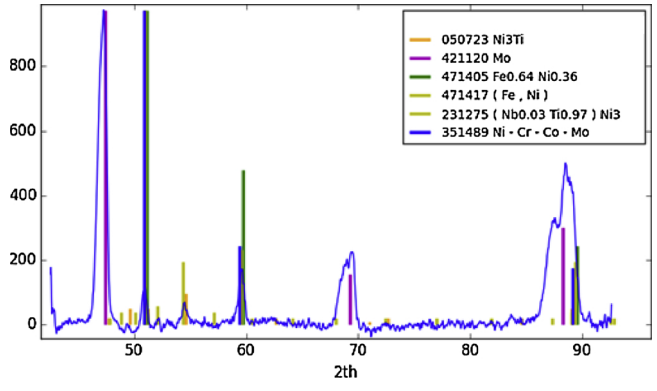

Fig. 15. X-ray crystallography of the 25 TA6V – 75 Mo / 30 Inconel 718 – 70 Mo interface.

Acknowledgments

The authors gratefully acknowledge the Labex Damas for its financial support and Julien GUYON, Olivier PERROUD, Etienne BRODU, Benoît BEAUSIR and Jean-Jacques FUNDENBERGER for fruitful discussions.

Appendix A. Supplementary data

Supplementary material related to this article can be found, in the online version, at doi:https://doi.org/10.1016/j.addma.2019.02.007.

References

[1] G. Hsiang Loh, E. Pei, D. Harrison, M.D. Monzón, An overview of functionally graded additive manufacturing, Addit. Manuf. 23 (2018) 34–44.

[2] L. Weiss, P. Acquier, L. Germain, D. Boisselier, E. Fleury, A. Hazotte, Microtexture developed during direct energy deposition of Ti-6Al-4V, Proceedings of the 13th World Conference on Titanium, (2016), pp. 1305–1310.

[3] S. Yin, X. Yan, C. Chen, R. Jenkins, M. Liu, R. Lupoi, Hybrid additive manufacturing of Al-Ti6Al4V functionally graded materials with selective laser melting and cold spraying, J. Mater. Process. Technol. 255 (2018) 650–655.

[4] R. Garcia, P. Prabhakar, Bond interface design for single lap joints using polymeric additive manufacturing, Compos. Struct. 176 (2017) 547–555.

[5] A. Bandyopadhyay, B. Heer, Additive manufacturing of multi-material structures, Mater. Sci. Eng. R 129 (2018) 1–16.

[6] C. Schneider-Maunoury, L. Weiss, P. Acquier, D. Boisselier, P. Laheurte, Functionally graded Ti6Al4V-Mo alloy manufactured with DED-CLAD process, Addit. Manuf. 17 (2017) 55–66.

[7] B. Onuike, A. Bandyopadhyay, Additive manufacturing of Inconel 718 – Ti6Al4V bimetallic structures, Addit. Manuf. 22 (2018) 844–851.

[8] B. Beausir, J.-J. Fundenberger, Analysis Tools for Electron and X-ray diffraction, ATEX-software, Université de Lorraine-Metz, 2017, www.atex-software.eu.

[9] B. Vrancken, L. Thijs, J.-P. Kruth, J. Van Humbeeck, Microstructure and mechanical properties of a novel β titanium metallic composite by selective laser melting, Acta

Mater. 68 (2014) 150–158.
[10] Y.S. Lee, M. Nordin, S.S. Babu, D.F. Farson, Influence of fluid convection on weld pool formation in laser cladding, Weld. J. 93 (2014) 292s–300s.
[11] A.K. Niessen, A.R. Miedema, F.R. de Boer, R. Boom, Enthalpies of formation of liquid and solid binary alloys based on 3d metals, Physica B 152 (1988) 303–346.
[12] J.L. Murray, Handbook Volume 3 – Alloy Phase Diagrams, ASM, 1992.
[13] J.-C. Crivello, R. Souques, A. Breidi, N. Bourgeois, J.-M. Joubert, ZenGen, a tool to generate ordered configurations for systematic first-principles calculations, the Cr-Mo-Ni-Re system as a case study, CALPHAD: Comput. Coupling Phase Diagr. Thermochem. 51 (2015) 233–240.
[14] K. Otsuka, X. Ren, Physical metallurgy of Ti-Ni-based shape memory alloys, Prog. Mater. Sci. 50 (2005) 511–678.
[15] K. Shah, I.U. Haq, S.A. Shah, F.U. Khan, M.T. Khan, S. Khan, Experimental study of direct laser deposition of Ti-6Al-4V and inconel 718 by using pulsed parameters, Sci. World J. (2014).